Desalination and Water Treatment
www.deswater.com
doi: 10.1080/19443994.2015.1014860

57 (2016) 6981–6990
March

Taylor & Francis
Taylor & Francis Group

Kinetics and mechanism study on adsorption of cadmium by freshly synthesized hydrous manganese dioxide

Yujia Zhai[a], Hongjie Wang[a,b,*]

[a]*College of Environmental Science and Engineering, Beijing Forestry University, Beijing 100083, P.R. China, Tel. +86 10 6233 6900; email: qingpu2005@126.com (Y. Zhai), huanjinglou105@126.com (H. Wang)*
[b]*Beijing Key Lab for Source Control Technology of Water Pollution, Beijing 100083, P.R. China*

Received 4 July 2014; Accepted 20 January 2015

ABSTRACT

Hydrous manganese dioxide (HMO) was synthesized by redox reaction of potassium permanganate ($KMnO_4$) and hydrogen peroxide (H_2O_2), and then freshly synthesized HMO (FSHMO) was used for cadmium (Cd(II)) removal from aqueous solutions. The specific surface area and the maximum adsorption capacity of FSHMO for Cd(II) are 127.46 $m^2\ g^{-1}$ and 168.36 mg g^{-1} at 298 K. The adsorption equilibrium can be well described by the Langmuir isotherm model and the adsorption capacity of FSHMO is higher than most of the average materials. The calculated theromodynamic parameters indicate a spontaneous and endothermic adsorption process. The pseudo-second-order equation gives a good fit for the adsorption process, and the calculated adsorption activation energy (E_a) is 48.68 kJ mol^{-1}. The uptake of Cd(II) by FSHMO is mainly attributed to the chemisorption. The velocities of film diffusion process and mass transfer process of Cd(II) on FSHMO are rapid enough, while the intraparticle diffusion process is the rate-limiting step for the uptake of Cd(II). The speciation of Cd(II) on the surface of FSHMO is close to $Cd(OH)_2$, but there is no formation of the new solid phase of $Cd(OH)_2$. In general, FSHMO is a promising candidate for Cd(II) removal from aqueous solutions.

Keywords: Adsorption; Heavy metal; Kinetics; Manganese dioxide; Mechanism

1. Introduction

Cadmium (Cd(II)) can enter the food chain through drinking water and crop irrigation [1]. Due to its acute toxicity, carcinogenic properties, non-biodegradability, and bioaccumulation, Cd(II) has joined in the most toxic category of heavy metals with the greatest potential hazard to humans and the environment [2]. It is necessary to develop effective technologies to remove Cd(II) from aqueous solutions.

Traditional processes, such as chemical precipitation [3], ion exchange [4], reverse osmosis [5], adsorption [6], and dialysis–electrodialysis [7], have been tested for the effective removal of toxic metals from water or wastewater. Especially, the adsorption process stands out for its rapidness and cost-effectiveness [8]. To develop a more efficient and economical process, a variety of natural minerals, waste biomass, and artificially synthesized materials have been used for the removal of metals [9]. With chemical activation by zinc chloride, Cronje et al. [10] synthesized an adsorbent from sugarcane bagasse for Cr(VI)

*Corresponding author.

adsorption, as well as Acharya et al. [11] developed a kind of tamarind wood-based activated carbon for the removal of Pb(II). Hydrous metal oxides, such as hydrous ferric oxide [12], hydrous manganese dioxide (HMO), nano-sized aluminum [13], titanium, zinc, magnesium, cerium oxides [14], show great talent in scavenging Cd(II) from aqueous solutions. In particular, HMO, due to its high surface charge [8], low cost, and availability, has demonstrated to be an excellent adsorbent to remove trace heavy metals from water and has become the focus of attention of many studies since the 1960s [15]. In the present field, the performance of the pre-prepared HMO [16], HMO-loaded materials [17], manganese dioxides formed *in situ* (MOF) [18], and MOF-loaded materials [19] in the removal of heavy metals has been studied in detail. Unfortunately, the pre-prepared HMO will suffer from relatively low adsorption capacity and poor selectivity [17], and the HMO-loaded materials will inevitably produce much more heavy metal-bearing residues. Although the MOF shows a promising ability in remedy of heavy metal-contaminated water [18], the potential risk that arises by pouring the oxidants and/or reducing agents directly into the water system and the convenience of operation need to be further considered.

The objectives of the work are: (a) to develop a kind of freshly synthesized hydrous manganese oxides and to characterize the structure of the materials and; (b) to evaluate the adsorption behavior of the materials for Cd(II) removal in aqueous solutions, and to explore the adsorption mechanism preliminarily.

2. Materials and methods

2.1. Materials

All chemicals, such as cadmium nitrate ($Cd(NO_3)_2{\cdot}4H_2O$), hydrogen peroxide (H_2O_2), potassium permanganate ($KMnO_4$), sodium hydroxide (NaOH), and hydrogen nitrate (HNO_3), were analytical grade and were purchased from Beijing Chemical Co. (Beijing, China). The Cd(II) stock solutions were prepared by dissolving $Cd(NO_3)_2{\cdot}4H_2O$ in appropriate amounts of deionized water. The concentrations of Cd(II) were always given as elemental cadmium concentration.

2.2. Adsorbent preparation

The HMO is freshly synthesized according to the previous works [20–22]. The main differences from the previous works are: (a) no ultrasound irradiation and no inert gas protection during the reaction and; (b) no drying process was conducted and the freshly synthesized adsorbent was dosed in 30 min without further treatment. The revised procedures are as follows. At 298 K, 1.816 g of $KMnO_4$ is dissolved in 100 mL of deionized water under vigorous magnetic stirring. Then, 30 mL of H_2O_2 (30%) is added dropwise into the $KMnO_4$ solution with addition of 0.1 M HNO_3 to keep the solution pH at 7.0 ($\pm$0.02). After addition of H_2O_2, the reaction went on for another 5 min. Such formed deep-brown suspension is identified as freshly synthesized hydrous manganese dioxide (FSHMO). After the reaction, a certain volume of FSHMO is injected directly into the solutions with preset concentration of Cd(II) for 0.5 h. Another 2 mL of the suspension is passed through a 0.45 μm membrane and the cake is digested by HNO_3. Then, the content of Mn is analyzed at wavelengths of 279.5 and 279.8 nm by an atomic adsorption spectrophotometer (AAS, AA-6300 Shimadzu Co., Acetylene air burner: 100 mm; Nitrous oxide acetylene flame head: 50 mm; Ignition dynamic baseline drift: ≤0.006A 30 min^{-1}; Related standard deviation of the accuracy: ≤0.5%). The concentration of such synthesized FSHMO is calculated as 4 mg mL^{-1} according to the concentration of Mn.

2.3. Characterization

The freeze-dried samples of FSHMO are characterized using several characterization techniques, including scanning electron microscopy (SEM, S-3000N Hitachi Co.), transmission electron microscopy (TEM, H-7500 Hitachi Co.), X-ray powder diffraction (X'Pert PRO MPD), and Fourier transform infrared spectroscopy (FT-IR, Nicolet 5700). Nitrogen (N_2) adsorption–desorption isotherms of the sample are measured by Brunauer–Emmett–Teller method (ASAP 2000, Micrometrics Co.), and the chemical analysis on the surfaces of the adsorbent is conducted by X-ray photoelectron spectroscopy (XPS, Kratos AXIS Ultra, UK) with a monochromator (Al Kα, hν = 1486.71 eV) or a dual anode (Al–Mg target).

2.4. Batch adsorption experiments

To investigate the influence of pH on Cd(II) adsorption, experiments are carried out by adding 2.5 mL of FSHMO sample into 100 mL of Cd(II) solutions with initial concentration of 20 mg L^{-1}. The pH conditions (2.0, 3.0, 4.0, 5.0, 6.0, and 7.0) are selected and the pH is adjusted every 2 h with 0.1 M HNO_3 or NaOH solution during the shaking process to designated values. After the reaction, all of the samples are filtered by a 0.45 μm film and the Cd(II) concentration of the filtrates are analyzed by an AAS at the wavelength of 228.8 nm.

To evaluate the effect of ionic strength on Cd(II) adsorption, 100 mL of 20 mg L^{-1} Cd(II) solutions at ionic strength ranged from 0.001 to 0.1 mol L^{-1} are prepared with $NaNO_3$, in 250 mL conical flasks. Other procedures are the same as those in the pH effect experiments.

Adsorption isotherms are determined by batch tests. 100 mL of Cd(II) solutions are added into 250 mL conical flasks with initial Cd(II) concentrations varying from 5 to 40 mg L^{-1}. Hundred milligram per liter of FSHMO is added into the bottles and the solution pH is maintained at 7.0 (±0.02). The bottles are shaken on at 140 rpm for 24 h at 288, 298, and 308 K, respectively. After the reaction, all samples are filtered by a 0.45 μm film and the Cd(II) concentration of the filtrates are analyzed by an AAS at the wavelength of 228.8 nm.

The kinetic experiments are carried out at 288, 298, and 308 K. The initial Cd(II) concentration is 20 mg L^{-1} and the dosage of FSHMO is 100 mg L^{-1}. The solution pH is adjusted to 7.0 (±0.02) by adding 0.1 M HNO_3 and/or NaOH and the agitation speed is fixed at 140 rpm. 5 mL of solutions are extracted from the suspension at various time intervals (0.1–24 h). All samples are filtered by a 0.45 μm film and the Cd(II) concentration of the filtrates are analyzed by an AAS at the wavelength of 228.8 nm.

The uptake of Cd(II) at time t (q_t) is calculated using the equation as follows:

$$q_t = \frac{V(C_0 - C_t)}{W} \tag{1}$$

where C_0 (mg L^{-1}) is the initial concentration of Cd(II) in solution, C_t (mg L^{-1}) is the concentration of Cd(II) in solution at time t, W (g) is the weight of FSHMO, and V(L) is the volume of the solution.

2.5. Modeling of adsorption isotherm and kinetics

The experimental results are fitted for using Langmuir [23] (Eq. (2)) and Freundlich isotherm models [24] (Eq. (3)), respectively.

$$q_e = \frac{q_{\max} K_L C_e}{1 + K_L C_e} \tag{2}$$

$$q_e = K_F C^{1/n} \tag{3}$$

where q_e is the equilibrium amount of Cd(II) adsorbed on FSHMO (mg g^{-1}); $q_{\max}$ is the maximum amount of Cd(II) adsorbed (mg g^{-1}); C_e is the equilibrium concentration of Cd(II) (mg L^{-1}); K_L is the Langmuir adsorption constant (L mg^{-1}); and K_F ((mg g^{-1})(L $mg^{-1})^{1/n}$) and n are the Freundlich adsorption isotherm constants.

The thermodynamic parameters of the adsorption process including Gibbs free energy (ΔG), enthalpy (ΔH), and entropy (ΔS) are also calculated according to the following equations:

$$\Delta G = -RT \ln\left(\frac{q_e}{C_e}\right) \tag{4}$$

$$\Delta G = \Delta H - T\Delta S \tag{5}$$

$$\ln\left(\frac{q_e}{C_e}\right) = \frac{\Delta S}{R} - \frac{\Delta H}{RT} \tag{6}$$

where R is gas constant (8.314 J (K mol)$^{-1}$) and T (K) is the temperature.

The pseudo-first-order Eq. (7) and pseudo-second-order kinetic model equations Eq. (8) are represented by the Lagergren equation [25] as given below:

$$\log\,(q_e - q_t) = \log\,(q_e) - \frac{K_1 t}{2.303} \tag{7}$$

$$\frac{t}{q_t} = \frac{1}{K_2 q_e{}^2} + \frac{t}{q_e} \tag{8}$$

where K_1 and K_2 (g (mg min)$^{-1}$) are the rate constants of pseudo-one-order and second-order equation, respectively, q_t is the same as Eq. (1), and t is the time (h).

Elovich equation [26] is commonly used in the kinetics of chemisorption of gas-state and liquid-state sorption on solids. The linear form of the simplified Elovich equation is given as follows:

$$q_t = \frac{\ln\,(\alpha\beta)}{\beta} + \frac{\ln\,t}{\beta} \tag{9}$$

where α is the initial sorption rate of Elovich equation (mg (g min)$^{-1}$), and the parameter β is related to the extent of surface coverage and activation energy for chemisorptions (g mg^{-1}). The constants can be obtained from the slope and the intercept of a straight line of q_t vs. ln t.

Mass transfer [27] study is carried out using the following equation:

$$\ln\left(\frac{C_t}{C_0} - \frac{1}{1 + mK_L}\right) = \ln\frac{mK_L}{1 + mK_L} - \frac{1 + mK_L}{mK_L}\beta_1 S_s t \tag{10}$$

where K_L is the Langmuir constant, m is the mass of the adsorbent per unit volume of particle-free adsorbate solution (g L^{-1}), which is given by $m = W/V$, S_s is the outer surface of the adsorbate per unit volume of particle-free slurry (cm), and β_1 (cm s^{-1}) is the external mass transfer coefficient.

Since the Elovich and pseudo-order kinetic models are unable to clarify the diffusion mechanism of the adsorption process, the intraparticle diffusion model [28] is used to determine the rate-limiting step of the adsorption kinetics. It is expressed as:

$$q_t = k_t^{1/2} + C \tag{11}$$

where q_t and t are the same as Eq. (1) and K is the rate constant for intraparticle diffusion (mg g^{-1} $h^{1/2}$).

3. Results and discussion

3.1. Adsorbent characterization

The results of N_2 adsorption–desorption isotherms and zeta potential experiments are illustrated in Fig. 1. All of the plots exhibit type IV isotherms with H1 hysteresis loop type according to the International Union of Pure and Applied Chemistry, which is the typical characteristic of mesoporous structure [26]. With the prolonged aging time, the inflection point shifts to lower partial pressure corresponding to the decrease of the pore diameter of the mesoporous materials. The values of specific surface area are 129.38 m^2 g^{-1}, 127.50 m^2 g^{-1}, 116.42 m^2 g^{-1}, and 87.24 m^2 g^{-1} with aging time prolonged from 0 to 8 h. Meanwhile, the values of point of zero charge (pH_{pzc}) maintain almost the same level (pH_{pzc} = 3.1) during the initial 2 h. To minimize the negative effect of aging time, FSHMO is dosed within 0.5 h after preparation.

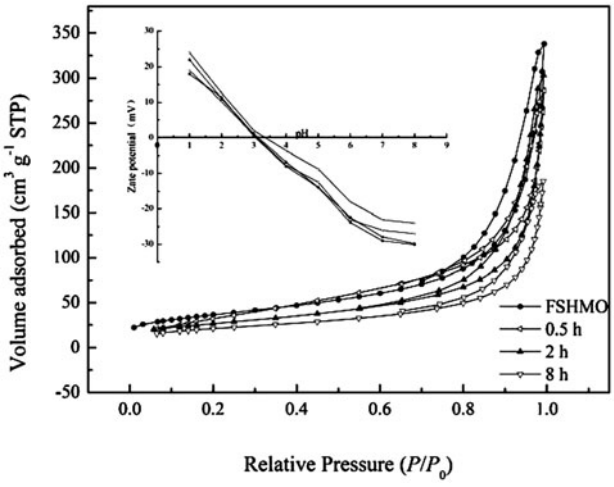

Fig. 1. N_2 adsorption/desorption isotherms and the corresponding zeta potential of the FSHMO at different aging times: 0, 0.5, 2, and 8 h.

As observed by SEM, the particle size of the clumps formed by spherical FSHMO nanoparticles is <200 nm (Fig. 2(a)), which is resembled as the reported materials [29]. The TEM image (Fig. 2(b)) presents the disordered mesoporous structure of FSHMO. The pore size is estimated to be 12 nm, which is slightly lower than the calculated results using BJH method.

3.2. Effect of pH and ionic strength

The effect of pH and ionic strength on Cd(II) removal are evaluated and the results are illustrated in Fig. 3. The Cd(II) removal efficiency increases steadily with the increase of solution pH from 2.0 to 7.0 and the maximum adsorption removal efficiency

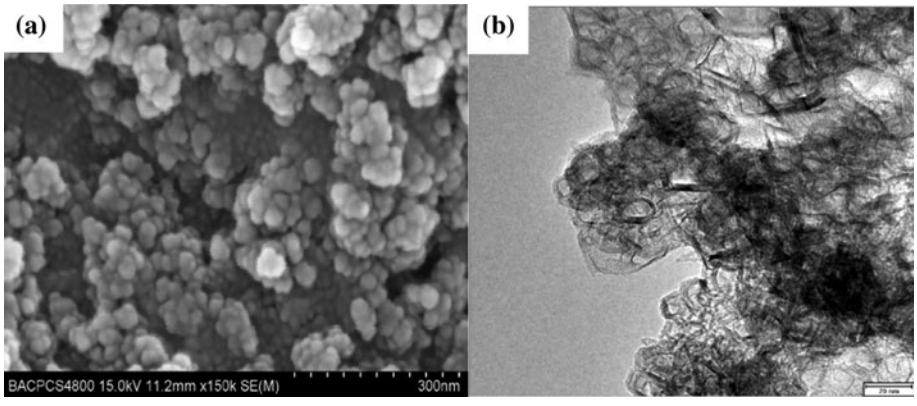

Fig. 2. SEM (a) and TEM (b) images of the FSHMO.

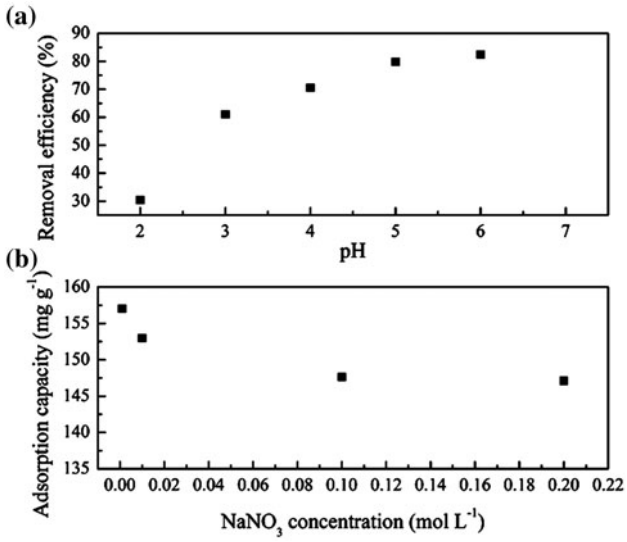

Fig. 3. (a) Effect of pH on Cd(II) removal: FSHMO, 100 mg L^{-1}; Cd(II), 20 mg L^{-1}; and T, 298 K; and (b) Effect of ionic strength on Cd(II) removal; pH 7.0; Cd(II), and 20 mg L^{-1}.

(82.4%) is acquired at pH 7.0. To avoid the negative effect of precipitation (pH > 8.0) [30], the adsorption experiments are conducted at pH 7.0. Meanwhile, the level of ionic strength has negligible effect on adsorption capacity, which indicates the adsorption of Cd(II) on FSHMO is ionic strength independent and the adsorption mechanism of Cd(II) is inner-sphere complexation, rather than ion exchange [31].

3.3. Effect of adsorbent dosage

The effect of FSHMO dosage on the adsorption percentage and the residual Cd(II) concentration in the solutions are shown in Fig. 4. With the increase of dosage from 0 to 7.5 mg L^{-1}, the residual Cd(II) concentration in the solutions decreases dramatically from 0.1 to 0.004 mg L^{-1}. There is a little increase in the removal efficiency by dosing extra adsorbent and the lowest residual Cd(II) concentration is 0.003 mg L^{-1} with 12.5 mg L^{-1} of FSHMO. After treated by FSHMO, the residual Cd(II) concentration in the solutions is < the limit of drinking water in China (≤ 0.005 mg L^{-1}), which demonstrates the potential ability of FSHMO in drinking water purification from Cd(II)-polluted water.

3.4. Adsorption isotherms

Isotherm studies are crucial to determine the maximum adsorption capacity (q_{max}) of Cd(II) onto FSHMO and the results are illustrated in Fig. 5. The

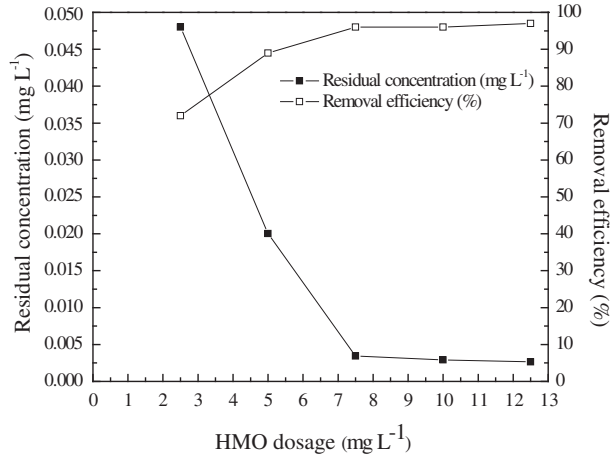

Fig. 4. Effect of the dosage on Cd(II) removal; pH 7.0; Cd (II), 0.1 mg L^{-1}; T, 298 K; and 24 h.

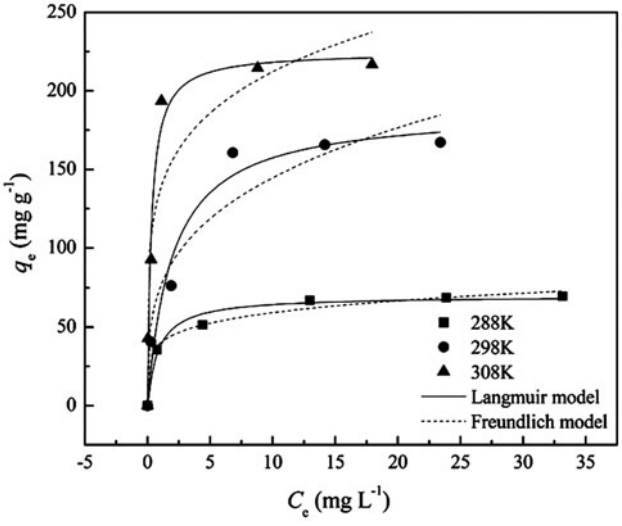

Fig. 5. Adsorption isotherms of Cd(II) removal at different temperatures: FSHMO, 100 mg L^{-1}; pH 7.0; Ionic strength, 0.01 mol L^{-1} $NaNO_3$; and 24 h.

experimental data are fitted by the Langmuir and Freundlich equations and the isotherm parameters are presented in Table 1. The values of coefficient of determination (R^2) indicate that the Langmuir model (R^2 = 0.987) gives a better fit for the experimental data than that of the Freundlich model (R^2 = 0.867). The q_{max} calculated by Langmuir model is consistent with the experimental equilibrium adsorption capacity (q_{exp}).

Besides, the comparison in specific surface area and maximum adsorption capacities between FSHMO and other reported adsorbents are listed in Table 2. The performance of FSHMO is almost at the same

Table 1
Isotherm, kinetic parameters, and q_{exp} for the adsorption system

Models and parameters		FSHMO		
		288 K	298 K	308 K
q_{exp} (isotherm)	mg g^{-1}	69.60	167.23	216.76
Langmuir equation				
K_L	L mg^{-1}	16.26	24.05	41.40
q_{max}	mg g^{-1}	82.08	168.36	224.74
R^2		0.987	0.960	0.992
Freundlich equation				
K_F	(mg g^{-1})(L mg^{-1})$^{1/n}$	136.64	260.69	327.49
n		0.19	0.29	0.33
R^2		0.867	0.925	0.961
q_{exp} (kinetic)	mg g^{-1}	66.77	158.77	212.75
Pseudo-first-order equation				
K_1	g (mg $min)^{-1}$	0.967	0.828	0.751
q_e	mg g^{-1}	61.75	146.73	202.39
R^2		0.920	0.946	0.844
Pseudo-second-order equation				
K_2	g (mg $min)^{-1}$	0.00137	0.00613	0.0157
q_e	mg g^{-1}	67.50	161.27	215.69
R^2		0.992	0.996	0.994
Elovich equation				
α	mg (g $min)^{-1}$	39.67	88.07	158.48
β	mg (g $min)^{-1}$	8.948	23.06	0.014
R^2		0.885	0.894	0.789
Intraparticle diffusion				
K_1		23.552	29.328	11.346
K_2	mg g^{-1} $min^{1/2}$	1.069	2.365	1.355
K_3		0.111	0.165	0.040

Table 2
Comparison of the q_{max} and specific surface area of various adsorbents

Adsorbent	pH	q_{max} (mg g^{-1})	Specific surface area (m^2 g^{-1})	References
HMO	3.5–4.0	104	100.5	[16]
MOF	~5.0	176	–	[18]
δ-MnO_2	6.05	40.75	–	[9]
MnO_2-loaded D301 resin	5.5	77.88	–	[19]
Magnetic manganese dioxide (MMO)	7.0	67.33	–	[33]
manganese dioxide	7.0	< 100	83.5	[27]
FSHMO	7.0	168.36	127.5	This work

level as that of MOF, but higher than most of the others.

3.5. Thermodynamic analysis

The negative values of ΔG are −6.68, −7.88, and −9.53 kJ mol^{-1} at 288, 298, and 308 K, respectively, which determined a spontaneous adsorption process. The positive value of ΔS (142.8 J mol^{-1}) reflects the randomness at the solid–liquid interface during the adsorption of Cd(II) on FSHMO. Besides, the positive value of ΔH (34.55 kJ mol^{-1}) determines that the adsorption process is endothermic.

3.6. Adsorption kinetics and activation energy

The variation of the adsorbed Cd(II) on the FSHMO with prolonged contact time is shown in Fig. 6. The adsorption capacity of Cd(II) on the FSHMO increases sharply within the initial 2 h at different temperatures,

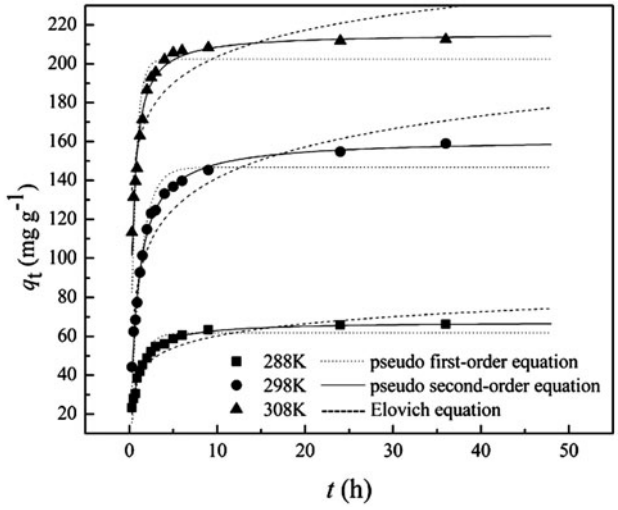

Fig. 6. Adsorption kinetics of Cd(II) at different temperatures: FSHMO, 100 mg L^{-1}; Cd(II), 20 mg L^{-1}; pH 7.0; and Ionic strength, 0.01 mol L^{-1} $NaNO_3$.

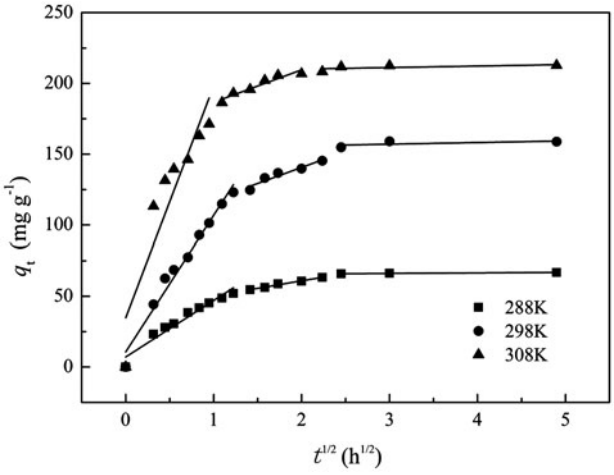

Fig. 7. Plots of q_t vs. $t^{1/2}$ for the intraparticle transport of Cd(II) onto FSHMO; pH 7.0; Cd(II), 20 mg L^{-1}; and Ionic strength, 0.01 mol L^{-1} $NaNO_3$.

then continues with a slower rate, and finally tends to reach equilibrium. Meanwhile, the temperature has an obvious positive effect on the uptake of Cd(II).

The parameters calculated according to the kinetic models are listed in Table 1. The value of the external mass transfer coefficient (β_1) is calculated to be 1.88×10^{-4} cm s^{-1}, which suggests that the velocity of mass transfer of Cd(II) on FSHMO is rapid enough [27]. The values of coefficient of determination ($R^2 > 0.99$) suggest that the pseudo-second-order model gives a good fit for the adsorption process, and the values of q_e are in accordance with that of the q_{exp}. It predominantly indicates the chemical adsorption of Cd(II) on FSHMO [32].

In order to further clarify the adsorption mechanism, the intraparticle diffusion model is used to determine the rate-limiting step of the adsorption process and the results are presented in Fig. 7. The multilinearity plots imply the external diffusion, intraparticle diffusion, and asdsorption equilibrium stages. Comparing the corresponding values of K_1, K_2, and K_3 for the stages in Table 1, the rate-limiting step of the adsorption process is ascribed to the intraparticle diffusion stage. Meanwhile, the line of the second step does not pass through the origin, which indicates that the rate of adsorption is controlled by the combination of intraparticle diffusion and the surface diffusion processes [28].

Arrhenius equation parameters are fitted by the rate constants simulated in pseudo-second-order kinetics to determine temperature-independent rate parameters and adsorption type. The value of the calculated activation energy (E_a) for Cd(II) adsorption onto FSHMO is 48.69 kJ mol^{-1}, which indicates that the chemical adsorption process dominates the adsorption process [34].

3.7. FTIR and XPS

The comparison of FTIR spectra of FSHMO before and after Cd(II) adsorption is illustrated in Fig. 8. The broad bands of hydroxyl groups at 3,410 and 1,630 cm^{-1} [35] are significantly shifted to 3,427 and 1,637 cm^{-1} and the peak at 1,637 cm^{-1} is strengthened after Cd(II) loading. Besides, the occurrence of the

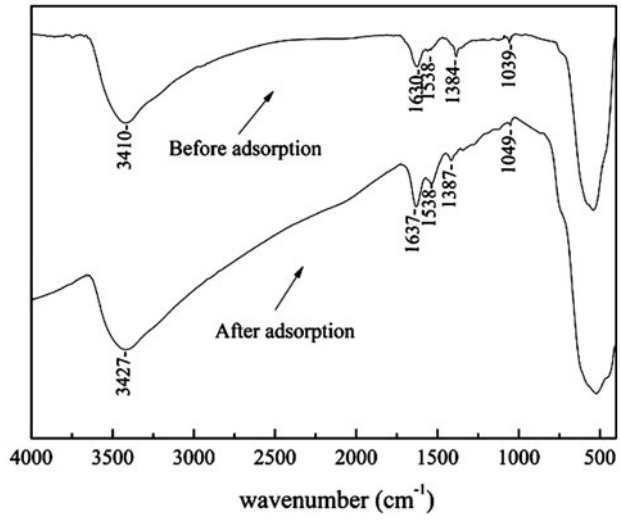

Fig. 8. FTIR spectra of FSHMO before and after Cd(II) adsorption.

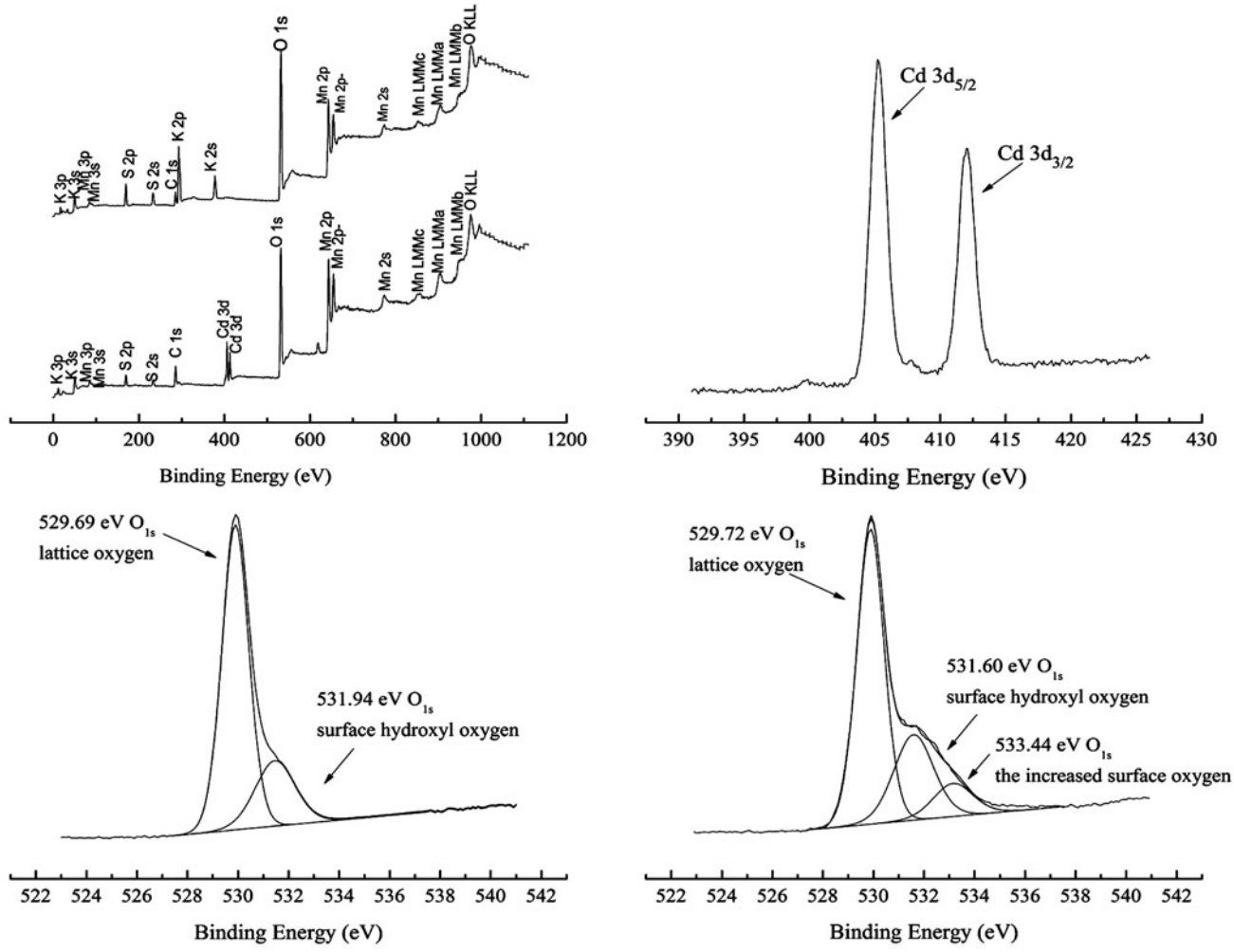

Fig. 9. XPS wide scan for FSHMO before and after Cd(II) adsorption (a); XPS detailed spectra of (b) Cd 3d; (c) O 1s before Cd(II) adsorption; and (d) O 1s after Cd(II) adsorption.

peaks at 1,039 and 1,538 cm^{-1} is attributed to the metal hydroxyl groups and the peaks are also strengthened after Cd(II) uptake [36]. It indicates that the adsorption could occur through the interaction between Cd(II) and the surface hydroxyl groups [37].

In order to further explore the mechanism of Cd(II) adsorption, XPS analysis of FSHMO before and after Cd(II) loading is conducted. The banding energies of Mn 2p are 642.61 and 642.40 eV before and after Cd(II) adsorption, which indicate the FSHMO is mainly in the form of MnO_2 [38]. The strong peaks of Cd appeared (Fig. 9(a)) after Cd(II) adsorption and the peaks at 411.63 and 404.80 eV (Fig. 9(b)) are assigned to Cd $3d_{3/2}$ and Cd $3d_{5/2}$ [39], which confirms the uptake of Cd(II). The banding energy of Cd $3d_{5/2}$ in $Cd(NO_3)_2$ is 406.66 eV, while a remarkable shift of the value (404.80 eV) is observed after Cd(II) adsorption. Moreover, the value of the banding energy of Cd $3d_{5/2}$ acquired in the test is close to the values reported for $Cd(OH)_2$ [40], which indicates the possible specific interaction between Cd(II) and the FSHMO [41]. The high-resolution XPS spectra of O 1s before and after Cd(II) loading are shown in Fig. 9(c) and (d), respectively. The peaks at banding energies of 529.69 and 529.72 are assigned to the lattice oxygen of virgin and Cd(II)-loaded FSHMO, meanwhile the peaks at banding energies of 531.94 and 531.60 eV are ascribed to the metal surface hydroxyl groups, respectively [42]. It is reported that the banding energy of O 1s in $Cd(OH)_2$ is 530.90 or 532.50 eV [43], which is much different from the result in Fig. 9(d). It demonstrates that there is no formation of the new solid phase of $Cd(OH)_2$. Meanwhile, the uptake of Cd(II) is correlated with the increase of the content of metal surface hydroxyl groups, which is in accordance with the FTIR results.

4. Conclusions

The FSHMO presents the disordered amorphous mesoporous structure. The Langmuir isotherm model could fit well for the experimental results and the maximum equilibrium adsorption capacities of FSHMO are 82.08, 168.36, and 224.74 mg g^{-1} at 288, 298, and 308 K, respectively. The maximum adsorption capacity of FSHMO for Cd(II) are on close to that of MOF, but higher than most of the other adsorbents. The pseudo-second-order equation describes the adsorption process well. Chemisorption dominated the adsorption process and the value of the calculated adsorption activation energy (E_a) is 48.68 kJ mol^{-1}. The velocities of film diffusion process and mass transfer process of Cd(II) are rapid enough, while the intraparticle diffusion process is the rate-limiting step for the uptake of Cd(II). The speciation of Cd on the surface of FSHMO is close to $Cd(OH)_2$, but there is no formation of the new solid phase of $Cd(OH)_2$. In general, the freshly synthesized hydrous manganese oxide is a promising candidate for Cd(II) removal from aqueous solutions.

Acknowledgments

This work was supported by the Fundamental Research Funds for the Central Universities [grant number TD2011-24] and the National Natural Science Research Fund [grant number 51278051].

List of symbols:

Symbols	Meaning	Unit
C_0	initial concentration of Cd (II) in solution	mg L^{-1}
C_t	concentration of Cd(II) in solution at time t	mg L^{-1}
V	volume of the solution	L
W	weight of FSHMO	g
q_e	equilibrium amount of Cd (II) adsorbed on FSHMO	mg g^{-1}
q_{max}	maximum amount of Cd (II) adsorbed	mg g^{-1}
C_e	equilibrium concentration of Cd(II)	mg L^{-1}
K_L	Langmuir adsorption constant	L mg^{-1}
K_F	Freundlich adsorption isotherm constants	(mg g^{-1})(L $mg^{-1})^{1/n}$
n	Freundlich adsorption isotherm constants	
q_t	amount of Cd(II) adsorbed at time t	mg g^{-1}
K_1	rate constant of pseudo one-order equation	g (mg min)$^{-1}$
K_2	rate constant of pseudo second-order equation	g (mg min)$^{-1}$
α	initial sorption rate of Elovich equation	mg (g min)$^{-1}$
β	extent of surface coverage and activation energy for chemisorptions	g mg^{-1}
S_s	outer surface of the adsorbate per unit volume of particle-free slurry	cm
m	the mass of the adsorbent per unit volume of particle-free adsorbate solution	g L^{-1}
β_1	external mass transfer coefficient	cm s^{-1}
K	rate constant for intraparticle diffusion	mg g^{-1} $h^{1/2}$
ΔG	Gibbs free energy	kJ mol^{-1}
ΔH	enthalpy	kJ mol^{-1}
ΔS	entropy	J mol^{-1}
R	gas constant	J (K·mol)$^{-1}$
E_a	activation energy	kJ mol^{-1}

References

[1] E.I. Unuabonah, K.O. Adebowale, B.I. Olu-Owolabi, L.Z. Yang, L.X. Kong, Adsorption of Pb(II) and Cd(II) from aqueous solutions onto sodium tetraborate-modified Kaolinite clay: Equilibrium and thermodynamic studies, Hydrometallurgy 93 (2008) 1–9.
[2] G.A. Drasch, An increase of cadmium body burden for this century—An investigation on human tissues, Sci. Total Environ. 26 (1983) 111–119.
[3] E.R. Christensen, J.T. Delwiche, Removal of heavy metals from electroplating rinsewater by precipitation, flocculation and ultrafiltration, Water Res. 16 (1982) 729–737.
[4] A. Bhattacharya, C. Venkobachar, Removal of cadmium(II) by low cost adsorbents, J. Environ. Eng. 110 (1984) 110–122.
[5] M.A. Mazid, Mechanisms of transport through reverse osmosis membrane, Sep. Sci. Technol. 19 (1984) 357–373.
[6] S.S. Tripathy, J.L. Bersillon, K. Gopal, Adsorption of Cd^{2+} on hydrous manganese dioxide from aqueous solutions, Desalination 194 (2006) 11–21.
[7] L. Marder, G.O. Sulzbach, A.M. Bernardes, J.Z. Ferreira, Removal of Cd(II) and cyanide from aqueous solutions through electrodialysis, J. Braz. Chem. Soc. 14 (2003) 610–615.
[8] J. Cheng, G. Shao, H. Yu, J. Xu, Excellent catalytic and electrochemical properties of the mesoporous MnO_2 nanospheres/nanosheets, J. Alloys Compd. 505 (2010) 163–167.
[9] S.E. Bailey, T.J. Olin, R.M. Bricka, D.D. Adrian, A review of potentially low-cost sorbents for heavy metals, Water Res. 33 (1999) 2469–2479.
[10] K.J. Cronje, K. Chetty, M. Carsky, J.N. Sahu, B.C. Meikap, Optimization of chromium(VI) sorption potential using developed activated carbon from sugarcane bagasse with chemical activation by zinc chloride, Desalination 275 (2011) 276–284.

[11] J. Acharya, J.N. Sahu, C.R. Mohanty, B.C. Meikap, Removal of lead(II) from wastewater by activated carbon developed from tamarind wood by zinc chloride activation, Chem. Eng. J. 149 (2009) 249–262.
[12] N.N. Mallikarjuna, A. Venkataraman, Adsorption of Pb^{2+} ions on nanosized γ-Fe_2O_3 formation of surface ternary complexes on ligand complexation, Talanta 60 (2003) 139–147.
[13] R.R. Bell, G.C. Saunders, Cd(II) adsorption on hydrous aluminium (III) oxide: Effect of adsorbed polyelectrolyte, Appl. Geochem. 20 (2005) 529–536.
[14] S.S. Tripathy, S.B. Kanungo, Adsorption of Co^{2+}, Ni^{2+}, Cu^{2+} and Zn^{2+} from 0.5 M NaCl and major ion sea water on a mixture of δ-MnO_2 and amorphous FeOOH, J. Colloid Interface Sci. 284 (2005) 30–38.
[15] S.B. Kanungo, S.S. Tripathy, Rajeev, Adsorption of Co, Ni, Cu and Zn on amorphous hydrous manganese dioxide from complex electrolyte solutions resembling sea water in major ion content, J. Colloid Interface Sci. 269 (2004) 1–10.
[16] Q. Su, B. Pan, S. Wan, W. Zhang, L. Lv, Use of hydrous manganese dioxide as a potential sorbent for selective removal of lead, cadmium, and zinc ions from water, J. Colloid Interface Sci. 349 (2010) 607–612.
[17] Q. Su, B. Pan, B. Pan, Q. Zhang, W. Zhang, L. Lv, X. Wang, J. Wu, Q. Zhang, Fabrication of polymer-supported nanosized hydrous manganese dioxide (HMO) for enhanced lead removal from waters, Sci. Total Environ. 407 (2009) 5471–5477.
[18] Q. Qin, Q. Wang, D. Fu, J. Ma, An efficient approach for Pb(II) and Cd(II) removal using manganese dioxide formed *in situ*, Chem. Eng. J. 172 (2011) 68–74.
[19] Z. Zhu, H. Ma, R. Zhang, Y. Ge, J. Zhao, Removal of Cd(II) using MnO_2 loaded D301 resin, J. Environ. Sci. 19 (2007) 652–656.
[20] M. Xu, H. Wang, D. Lei, D. Qu, Y. Zhai, Y. Wang, Removal of Pb(II) from aqueous solution by hydrous manganese dioxide: Adsorption behavior and mechanism, J. Environ. Sci. 25 (2013) 479–486.
[21] H. Zhang, M. Xu, H. Wang, D. Lei, D. Qu, Y. Zhai, Adsorption of copper by aminopropyl functionalized mesoporous delta manganese dioxide from aqueous solution, Colloids Surf., A 435 (2013) 78–84.
[22] A. Abulizi, G.H. Yang, K. Okitsu, J. Zhu, Synthesis of MnO_2 nanoparticles from sonochemical reduction of MnO_4^- in water under different pH conditions, Ultrason. Sonochem. 21 (2014) 1629–1634.
[23] I. Langmuir, The constitution and fundamental properties of solids and liquids, J. Am. Chem. Soc. 38 (1916) 2221–2295.
[24] M.F. Freundlich, Over the adsorption in solution, J. Phys. Chem. 57 (1906) 385–470.
[25] K. Periasamy, C. Namasivayam, Process development for removal and recovery of cadmium from wastewater by a low-cost adsorbent: Adsorption rates and equilibrium studies, Ind. Eng. Chem. Res. 33 (1994) 317–320.
[26] S.H. Chien, W.R. Clayton, Application of Elovich equation to the kinetics of phosphate release and sorption in soils, Soil Sci. Soc. Am. J. 44 (1980) 265–268.
[27] M. Özacar, Equilibrium and kinetic modelling of adsorption of phosphorus on calcined alunite, Adsorption 9 (2003) 125–132.
[28] Y. Önal, C. Akmil-Başar, D. Eren, Ç. Sarıcı-Özdemir, T. Depci, Adsorption kinetics of malachite green onto activated carbon prepared from Tunçbilek lignite, J. Hazard. Mater. 128 (2006) 150–157.
[29] M. Singh, D.N. Thanh, P. Ulbrich, N. Strnadová, F. Štěpánek, Synthesis, characterization and study of arsenate adsorption from aqueous solution by α- and δ-phase manganese dioxide nanoadsorbents, J. Solid State Chem. 183 (2010) 2979–2986.
[30] Y. Xue, H. Hou, S. Zhu, Competitive adsorption of copper(II), cadmium(II), lead(II) and zinc(II) onto basic oxygen furnace slag, J. Hazard. Mater. 162 (2009) 391–401.
[31] D. Tiwari, C. Laldanwngliana, C.H. Choi, S.M. Lee, Manganese-modified natural sand in the remediation of aquatic environment contaminated with heavy metal toxic ions, Chem. Eng. J. 171 (2011) 958–966.
[32] H.K. Boparai, M. Joseph, D.M. O'Carroll, Kinetics and thermodynamics of cadmium ion removal by adsorption onto nano zerovalent iron particles, J. Hazard. Mater. 186 (2011) 458–465.
[33] C.A.C. Rosas, M. Franzreb, F. Valenzuela, W.H. Höll, Magnetic manganese dioxide as an amphoteric adsorbent for removal of harmful inorganic contaminants from water, React. Funct. Polym. 70 (2012) 516–520.
[34] H. Chen, J. Zhao, J. Wu, G. Dai, Isotherm, thermodynamic, kinetics and adsorption mechanism studies of methyl orange by surfactant modified silkworm exuviae, J. Hazard. Mater. 192 (2011) 246–254.
[35] Z. Liu, K. Ooi, H. Kanoh, W. Tang, X. Yang, T. Tomida, Synthesis of thermally stable silica-pillared layered manganese oxide by an intercalation/solvothermal reaction, Chem. Mater. 13 (2001) 473–478.
[36] R. Liu, H. Liu, Z. Qiang, J. Qu, G. Li, D. Wang, Effects of calcium ions on surface characteristics and adsorptive properties of hydrous manganese dioxide, J. Colloid Interface Sci. 331 (2009) 275–280.
[37] L. Xiong, C. Chen, Q. Chen, J. Ni, Adsorption of Pb(II) and Cd(II) from aqueous solutions using titanate nanotubes prepared via hydrothermal method, J. Hazard. Mater. 189 (2011) 741–748.
[38] C.D. Wagner, Photoelectron and auger energies and the auger parameter. in: D. Briggs, M.P. Seah (Ed.), Practical Surface Analysis: Auger and X-ray Photoelectron Spectroscopy, Wiley Publishers, New York, NY, 1990, pp. 595–610.
[39] F. Qin, B. Wen, X. Shan, Y. Xie, T. Liu, S. Zhang, S.U. Khan, Mechanisms of competitive adsorption of Pb, Cu, and Cd on peat, Environ. Pollut. 144 (2006) 669–680.
[40] O.P. Tkachenko, E.S. Shpiro, M. Wark, G. Schulz-Ekloff, N.I. Jaeger, X-ray photoelectron/X-ray excited auger electron spectroscopic study of highly dispersed semiconductor CdS and CdO species in zeolites, J. Chem. Soc. Faraday Trans. 89 (1993) 3987–3994.
[41] B. Pan, H. Qiu, B. Pan, G. Nie, L. Xiao, L. Lv, W. Zhang, Q. Zhang, S. Zheng, Highly efficient removal of heavy metals by polymer-supported nanosized hydrated Fe(III) oxides: Behavior and XPS study, Water Res. 44 (2010) 815–824.
[42] K.C.C. Kharas, J.H. Lunsford, Catalytic partial oxidation of methane over barium metaplumbate BaPbO3: Possible involvement of peroxide ion, J. Am. Chem. Soc. 111 (1989) 2336–2337.
[43] J.S. Hammond, S.W. Gaarenstroom, N. Winograd, X-ray photoelectron spectroscopic studies of cadmium- and silver-oxygen surfaces, Anal. Chem. 47 (1975) 2193–2199.